Tailoring hardness and electrochemical performance of TC4 coated Cu/a-C thin coating with introducing second metal Zr

Sara Khamseh, Eiman Alibakhshi, Bahram Ramezanzadeh, Jean-Sébastien Lecomte, Pascal Laheurte, Xavier Noirefalize, Fouad Laoutid, Henri Vahabi

Tailoring hardness and electrochemical performance of TC4 coated Cu/a-C thin coating with introducing second metal Zr

Sara Khamseh[1,*], Eiman Alibakhshi[2], Bahram Ramezanzadeh[2], Jean-Sébastien Lecomte[3], Pascal Laheurte[3], Xavier Noirefalize[4], Fouad Laoutid[4], Henri Vahabi[5,6,*]

[1] Department of Nanomaterial and Nanocoatings, Institute for Color Science and Technology, Tehran, Iran

[2] Surface Coating and Corrosion Department, Institute for Color Science and Technology, Tehran, Iran

[3] Universite de Lorraine, Laboratoire LEM3 UMR 7239, Metz, F-57045, France

[4] Laboratory of Polymeric and Composite Materials, Materia Nova Research Center, Avenue Copernic 1, 7000 Mons, Belgium

[5] Université de Lorraine, CentraleSupélec, LMOPS, F-57000 Metz, France

[6] Laboratoire Matériaux Optiques, Photoniques et Systèmes, CentraleSupélec, Université Paris-Saclay, 57070, Metz, France

To whom correspondence should be addressed:

* Sara Khamseh; khamseh-sa@icrc.ac.ir

* Eiman Alibakhshi; Alibakhshi-ei@icrc.ac.ir

* Henri Vahabi; henri.vahabi@univ-lorraine.fr

Abstract

The objective of this study was to develop multifunctional protective biocompatible (Cu, Zr)/a-C: H coatings with good mechanical properties and high corrosion resistance using a sputtering system on the surface of TC4 alloy. Coatings with a higher Zr/Cu ratio showed higher hardness, Young's modulus, and superior bio-corrosion resistance. It was demonstrated that charge transfer resistance of the coating with a higher Zr/Cu ratio enhanced from ~ 40 $k\Omega.cm^2$ to ~ 990 $k\Omega.cm^2$ after 168 h of immersion time. The results also showed strong synergistic effects of Cu and Zr, as well as the formation of the zirconium carbide phase on the surface.

Keywords: A. Sputtered films; A. Titanium; B. EIS; B. XPS; C. Passive films

1. Introduction

The development of high-performance materials like Titanium alloys for biomedical applications is an attractive topic of recent researches. Ti–6Al–4V (TC4) alloy is an inexpensive titanium alloy that has widespread applications, including biomedical applications [1,2] owing to its excellent mechanical properties at low and high temperatures. However, its uses are limited because of moderate hardness and wear strength, which causes debris containing toxic species at the surfaces of the prosthesis and implants.

To overcome these limitations, some protective coatings can be used [1,2,5,6]. Amorphous carbon thin coatings (a-C) refer to a class of amorphous carbon coatings containing a mixed structure of sp^3 and sp^2 bonds. The amorphous carbon thin coatings (a-C) are widely used as protective coatings owing to their outstanding properties such as chemical stability, high corrosion resistance, biocompatibility, excellent mechanical properties, and high wear resistance [7–12]. Recently, the metal-doped a-C thin coatings have made enormous progress in advanced applications [7,8,13–15]. The added metal to the thin carbon-based coatings can react with the carbon, forming the metal carbide or acting passive to the carbon layer [16–18]. Moreover, the metal incorporation improves the a-C thin coatings adhesion to the metal substrates, enhancing the graphitization of the coatings as well as the release of the internal stress [7,8]. None carbide metals such as Cu and Ni have been used to decrease the internal stress and control the corrosion resistance, wettability, and mechanical properties of the a-C thin coatings [7–9,16]. In contrast, the addition of carbide formed metals, namely Zr or Cr into a-C matrix, reduces the stress without any significant variation neither in hardness nor in the corrosion resistance [17,18].

Transition metals such as copper, zirconium, titanium, tantalum, and niobium are biocompatible [18-23]. Accordingly, the a-C thin coatings doped with these metals present a

synergistic behavior since they show improved adhesion and good biocompatibility. The Cu shows an excellent antibacterial effect and has a low cost compared to other antibacterial materials such as Ag and Au. Some works report the result of Cu addition on both mechanical and physical properties of the a-C thin coatings [7,8,19–21]. For example, it was reported that a-C thin coatings are containing higher Cu present high sp^2-bonded carbon with excellent antibacterial activity in addition to high biocompatibility [19,20]. Another research showed that the a-C thin coatings with higher Cu content show higher hardness and better adhesion to the metallic substrates [21,22].

On the other hand, the zirconium has also been used in biomedical applications for decades. Nowadays, a wide variety of treatments like implantology are using zirconium [23,24]. Zirconium shows excellent biocompatibility and mechanical properties in addition to high corrosion resistance [23,24]. It has been demonstrated that the Zr addition to the a-C thin coatings decreases the friction coefficient leading to a better wear resistance [25–27]. Bai et al. demonstrated that the Zr addition to the graphite-like carbon (GLC) improves the bio-corrosion resistance of the coatings [26].

Recently, it is shown that the a-C thin coatings doped with hard and soft metal (co-doped) could remarkably ameliorate the mechanical and tribological properties of the thin coatings [28–31]. It has been reported that the Ti/Al, Cr/Al, Cr/Cu, and Ti/Cu co-doped a-C thin coatings show better tribological properties, lower internal stress and strong adhesion to the metal substrates [28–31]. Liu et al. prepared Si/Al co-doped a-C thin coatings and revealed positive impacts of the co-doping process on the wear resistance and mechanical properties of the thin coatings [32,33]. Li et al. studied the Ti/Al co-doped amorphous carbon thin coatings and showed that the thin coating with low residual stress and high hardness were formed at an optimum Ti/Al ratio [34]. Wu et al. revealed that at an appropriate RF power, (F, Si) the co-doped a-C thin coatings show excellent mechanical properties and wear resistance [35].

Elsewhere, the Si/Ag co-doping caused high elastic recovery, good tribological properties, and high antibacterial rate in the a-C thin coatings [36]. Sun et al. demonstrated that the Cr and Cu co-doped a-C thin coatings show high hardness values caused by the formation and distribution of the hard chromium carbide nano-particles in the a-C matrix [37]. However, few efforts have been devoted to study the synergistic effect of the co-doped metals on the microstructure and properties of a-C thin coatings.

It is well-established that the mechanical and electrochemical properties of the protective coatings in the simulated body fluid can determine the biological performance of the surface coated biocompatible metals. For instance, it is well known that the wear rate of the a-C thin coatings can be predicted based on the hardness [38]. In contrast, since bio-engineering coatings are in contact with body fluids, the lifetime of the coated biocompatible metals can be determined based on the bio-corrosion resistance [21,39]. Bayón et al. reported the formation of Ti containing a-C coatings with appropriate adhesion and good corrosion resistance [40]. In another report, Azzi et al. showed that a SiN_x interlayer could improve the corrosion resistance of the a-C thin coating [11].

Based on the above discussion, synthesis and evaluation of the co-doped a-C thin coatings, including Cu and Zr, would be a beneficial step in the progress of high-performance biomedical coatings. To the best of the author's knowledge, there is no report on the synergistic effect of Cu and Zr on the microstructure and properties of the (Cu, Zr)/a-C thin coatings. It is well understood that the microstructure of the thin coating strongly affects its mechanical and electrochemical properties — an optimum microstructure result from the perfect design of the deposition condition of thin coatings [41]. The purpose of the present work is to address the synergistic effect of Cu and Zr on the mechanical properties and bio-corrosion resistance of (Cu, Zr)/a-C thin coatings prepared using a magnetron sputtering

system. It was attempted to find the best microstructure that guarantees excellent mechanical properties and high corrosion resistance in biological agents (SBF).

2. Experimental procedure

2.1. Sample preparation

Coatings were grown on the mirror-polished TC4 alloy and microscopic glass slide substrates using a planar type magnetron sputtering system, (Yarenikane Saleh-DRS320). The copper target was sputtered under a mixed atmosphere of argon and methane when the CH_4/Ar ratio fixed at 2.3. To add Zr into the Cu/a-C thin coating, the circular coupons of Zr with a diameter of 0.2 mm were set on the erosion track of the Cu target. The total number of Zr coupons varied from 1 to 5 to control the zirconium content of the coatings. The substrates were cleaned by ultrasonication in acetone, ethanol, and 2-propanol before placing them into the deposition chamber.

2.2. Characterization

The chemical composition of the deposited coatings was examined by an electron probe micro-analyzer (EPMA) device (JEOL, JXA-8530F). Raman analysis (Takram P50C0R10) was carried out to characterize the structure of the coatings. The exact composition of the (Cu, Zr)/a-C thin coatings was characterized using XPS (Al kα radiation at a pressure of 10^{-9} mbar, Thermo Fisher Scientific, USA).

The surface roughness of the prepared coatings was evaluated by atomic-force microscopy, Park Scientific Instrument (PC). The surface features of the coatings were studied using a field emission scanning electron microscopy (FE-SEM) (FE-SEM-model Tescan).

The internal stress value of the coatings was evaluated using a surface profile measuring instrument. The change of substrate curvature with coating's deposition was measured, and the coating internal stress was calculated using the Stoney equation [42]:

$$\sigma = [\frac{ET^2}{3(1-\vartheta)L^2t}]4\delta \quad (1)$$

E, ϑ, T, and L are Young's modulus, Poisson's ratio, substrate thickness, and substrate length, respectively.

Mechanical properties (hardness and Young's modulus) were measured using a Hysitron Inc. Tribo Scopes Nanomechanical Test Instrument. The indentation was performed using a Berkovich diamond indenter at room temperature. The load was selected to keep an impression depth not more than 10% of the film thickness so that the influence of the substrate could be neglected.

2.3.Electrochemical methods

The corrosion resistance of the TC4 alloy samples coated by various (Cu, Zr)/a-C thin coatings was investigated by electrochemical impedance spectroscopy (EIS) and polarization tests. These measurements were performed using an Ivium Compactstat power. The EIS test was conducted at room temperature (25±2 °C) and in a three-electrode cell, including Ag/AgCl (3 M KCl) as a reference, graphite rod as the counter, and the TC4 alloy samples, with and without coating, as the working electrode. The coated and uncoated TC4 alloy samples (1 cm^2) were dipped in a simulated body fluid (SBF) solution (the chemical composition of simulated body fluid (SBF) solution is given in **Table 1**) for 5, 24, 48, and 168 h. The test was done at open circuit potential (OCP), ±10 mV perturbation (peak-to-zero), and in the frequency range of 10 kHz-10 mHz. For each coating, three samples were tested to ensure reproducibility. The measured spectra were fitted using the ZDimpWin software.

The polarization test was performed after 168 h immersion in the range of -200 to 200 mV vs. Ag/AgCl around the open circuit potential OCP. For obtaining the polarization curves, a sweep rate of 0.5 mV/s was employed.

Table 1. Chemical composition of the SBF solution used for the EIS test [3].

Glucose	$Na_2HPO_2.2H_2O$	$MgSO_4.7H_2O$	KH_2PO_4	$MgCl_2.6H_2O$	$NaHCO_3$	$CaCl_2$	KCl	NaCl
1 g/L	0.1 g/L	0.06 g/L	0.1 g/L	0.48 g/L	0.35 g/L	0.18 g/L	0.4 g/L	8 g/L

3. Results and discussion

Raman spectroscopy was used to analyze the bonding structure and quality of Cu/a-C and (Cu, Zr)/a-C thin coatings. The Raman spectra of the (Cu, Zr)/a-C thin coatings are provided in **Fig. 1**. The variation of the Zr/Cu ratio of the coatings is presented in **Table 2**. It can be seen that introducing a few amounts of Zr strongly affects the structure of Cu/a-C thin coating. The Raman spectrum of the CZ-1 (Zr/Cu=0) and CZ-2 (Zr/Cu=0.4) samples contains two typical features of G (for graphite) and D (for disorder) bonds, which indicates the DLC (Diamond-Like Carbon) phase generation in the coatings [7, 47]. The G band corresponds to the highly ordered pyrolytic graphite, whereas D band corresponds to disorder in the graphite-like sp^2 bonding. The I_D/I_G ratio in a perfectly ordered pyrolytic graphite structure is zero. Therefore, this ratio can be considered as an indicative milestone to determine how far the carbon-based phase of the coatings is formed in a graphitic-structure framework [43]. The I_D/I_G ratio of the coatings is shown in **Table 2**. The I_D/I_G ratio in CZ-1 coating (Zr/Cu=0) is higher than the CZ-2 (Zr/Cu=0.4). Furthermore, the G peak position of the CZ-1 coating (Zr/Cu=0) is higher than that for the CZ-2 (Zr/Cu=0.4) coating. The decrease of the I_D/I_G ratio besides the shift of G peak position of the (Cu, Zr)/a-C thin coatings, induced by the

presence of few amounts of Zr, reveals the presence of a higher proportion of sp^3 bonded carbons and the increase of diamond-like domain size. There were no D and G peaks in (Cu, Zr)/a-C, the Raman spectra of the thin coatings containing higher Zr/Cu ratios (CZ-3 to CZ-6). In contrast, broad and diffused peaks observed, indicating that most of the carbon coating is in the amorphous state [44]. Here we can conclude that the increase in Zr content in the (Cu, Zr)/a-C thin coating breaks the long-range order of the graphitic structure.

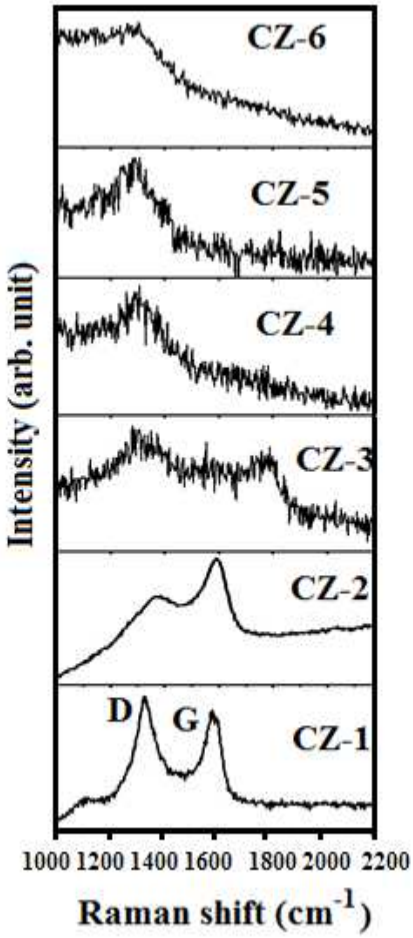

Fig 1. Raman spectrum of prepared samples in 1000–2200 cm^{-1} range.

FWHM (full width at half maximum) value of the D peak increased with increasing the Zr content and shifted to the lower wavenumbers. This is an indicator of the presence of disorder sp^2 network, a higher proportion of the sp^3 bonds and a bigger diamond domain size. In sum, the introduction of a low Zr content (Zr/Cu ratio of 0.4) leads to a higher proportion

of the sp^3 bonded carbons and the high Zr content (Zr/Cu=0.5-0.8) breaks the long-range order of the graphite structure and induces an increase of the diamond-like domain size. It has been shown that the incorporation of the metal encourages the formation of sp^2 bonded carbon sites [7,8,45,46]. In our previous study, it was revealed that the Cu/a-C thin coatings with higher Cu contents present a higher proportion of sp^2 bonded carbons and graphitic domain size [7,8]. However, it seems that the Cu and Zr co-doping affects the structure of the a-C coatings differently. The coating structure becomes a disorder with higher sp^3 bonding as a result of the synergistic effect of Cu and Zr [4,7].

Table 2. Details of chemical composition, roughness, and Raman parameters of (Cu, Zr)/a-C thin coatings.

Sample no	Zr (at%)	Zr/Cu ratio	Internal stress (GPa)	Roughness Rms (nm)	D peak position (cm^{-1})	G peak position (cm^{-1})	I_D/I_G
CZ-1	0	0	1.2±0.2	1	1387 D FWHM=218	1589 G FWHM=85	2.2
CZ-2	12	0.4	2±0.3	23	1366 D FWHM=250	1567 G FWHM=90	0.371
CZ-3	14	0.5	2.5±0.3	-	1306 D FWHM=56.836	1770 G FWHM=86.3	0.83
CZ-4	17	0.6	2.8±0.2	19	-	-	-
CZ-5	18	0.7	3.2±0.35	-	1306 D FWHM=113.8	-	-
CZ-6	22.58	0.8	3.5±0.32	9.5	1366 D FWHM=110.3	-	-

To better investigate the chemical state of C, Cu, and Zr in the coating surface, the XPS analysis was carried out. The deconvoluted XPS C1s spectra for the CZ-2 and CZ-5 coatings with Zr content of 12 and 18 at% are shown in **Fig. 2**. The C 1s spectrum was discrete into four peaks. The peak centered at 282.1 eV is contributed to the zirconium carbide (Zr-C bond) [25,47]. The three peaks at around 284.7, 285.2, and 288 eV are attributed to the sp^3-C, the sp^2-C, and C=O groups, respectively [37,48]. The abundance of each bonding estimated using the integral-area ratio of each peak from the Lorentzian curve fittings and results are shown in **Table 3**. It can be seen that the increase in the Zr content in the coatings resulted in the rise of the sp^3/sp^2 ratio and C-Zr content of (Cu, Zr)/a-C thin coatings. These results highlight that the high Zr content induces short-range order of (Cu, Zr)/a-C thin coatings, which matches well with Raman analysis results. Moreover, it can be seen that the zirconium carbide phase content of the coatings increased with the increasing Zr content.

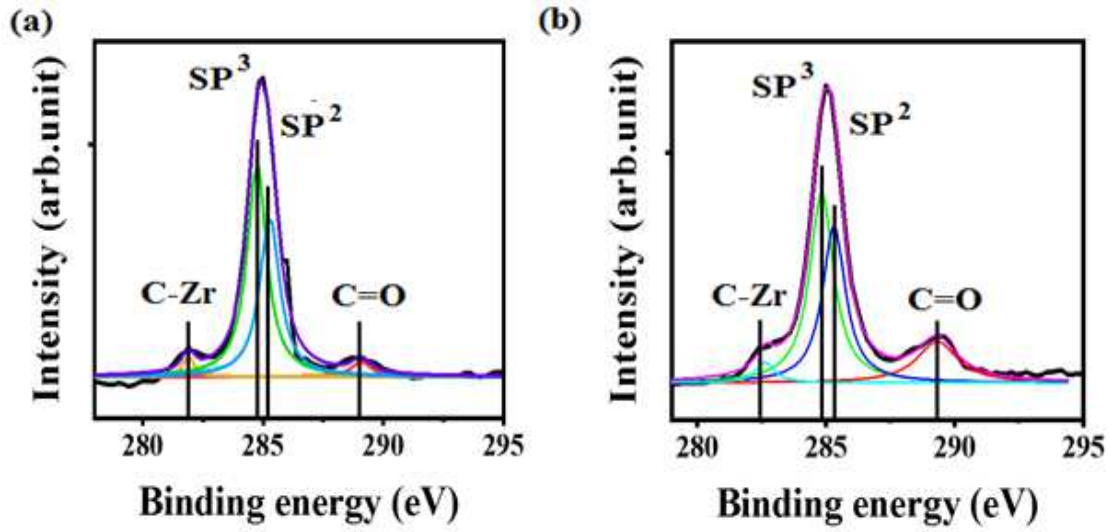

Fig 2. Deconvoluted C 1s XPS spectra of (a) CZ-2 and (b) CZ-5 coatings.

The Cu 2p and Zr 3d spectra of CZ-2 and CZ-5 coatings with Zr contents of 12 and 18 at% are shown in **Fig. 3(a-d)**. The Cu 2p spectra of both coatings are separated into two peaks, which are attributed to the Cu 2p 3/2 and Cu 2p 1/2, located at 952.6 eV for CZ-2, 950.8 eV for CZ-5 and 932.7 eV for CZ-2 and 930.4 eV for CZ-5, respectively [13]. No Cu-C bonding has been formed in the coatings. In contrast, the Zr 3d spectrum of both thin coatings contained two peaks at around 181.9 eV for CZ-2, 182.2 eV for CZ-5, and 184.3 eV for CZ-2, 184.6 eV for Cz-5 which are corresponding to Zr-C and ZrO_2, respectively. Here it can be concluded that the ZrC phase has been formed in both coatings (CZ-2 and CZ-5) when the coatings are partly oxidized as a result of the residual oxygen in the sputtering chamber during the coatings deposition [49]. Moreover, the small amount of oxygen is due to physical absorption when exposed to air.

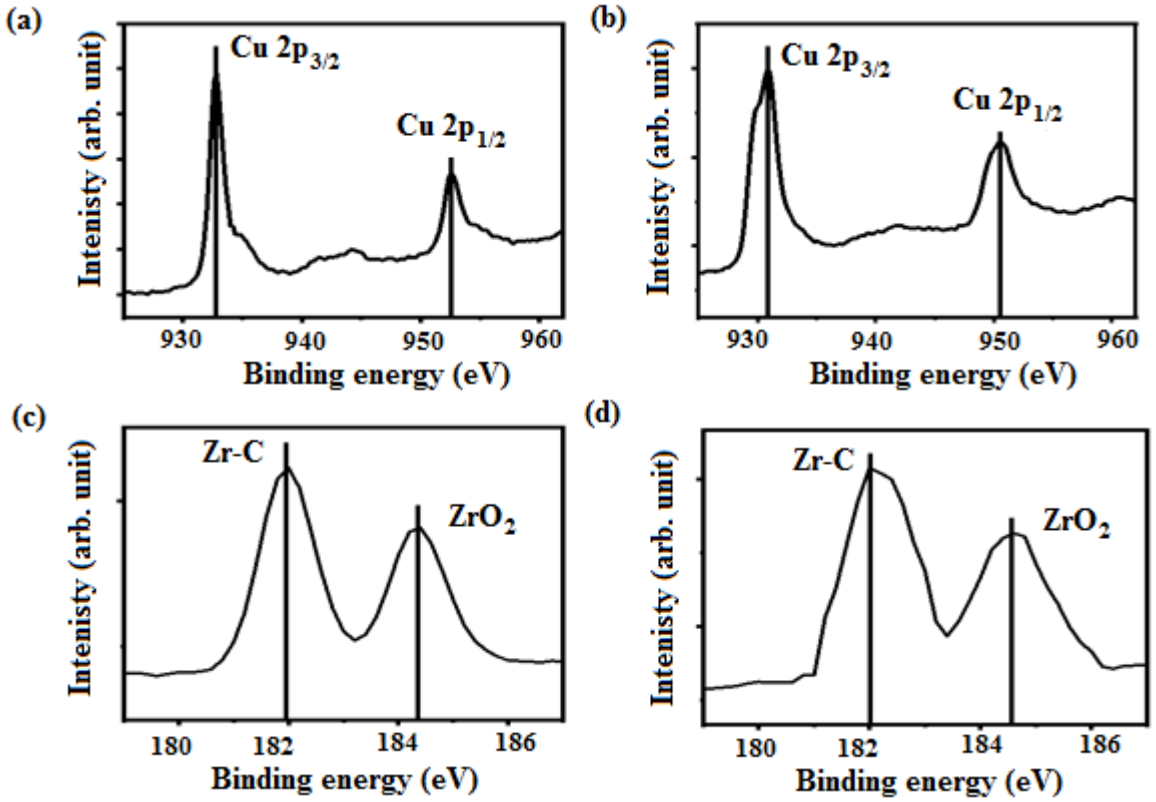

Fig 3. (a, b) Cu 2p XPS spectrum of CZ-2 and CZ-5 coatings, (c, d) Zr 3d XPS spectrum of CZ-2 and CZ-5 coatings.

Table 3. The bonding structure of CZ-2 and CZ-5 thin coatings obtained from C 1s XPS spectra.

Sample No	**Zr at%**	**sp^2 (%)**	**sp^3 (%)**	**sp^3/sp^2**	**($A_{(C-Zr)}/A_{(C1s)}$)**	**($A_{(C=O)}/A_{(C1s)}$)**
CZ-2	12	56.63	43.37	1.25	0.1	0.01
CZ-5	18	57.7	44.3	1.32	0.13	0.04

A: The peak area

SEM and AFM micrographs were performed to determine the morphology and surface roughness of both Cu/a-C and (Cu, Zr)/a-C thin coatings. Plane view FE-SEM image of CZ-1 coating with no Zr (**Fig. 4(a)**) depicts the development of a smooth surface when some round grains formed on the surface. This kind of morphology has been reported previously for the immiscible metal/carbon thin coatings such as Cu/a-C thin coatings [7,8]. In CZ-2 coating with the lowest Zr/Cu ratio (**Fig. 4(b)**), a pebble-like structure with open grain boundaries and defective structure has been developed. The surface morphology of the CZ-4 coating with a Zr/Cu ratio of 0.6 is almost the same as the CZ-2 coating (**Fig. 4(c)**). However, the coating density of the CZ-4 coating is higher when its defects density is lower than that of CZ-2 coating. A flake-like morphology with low defect density was observed in the CZ-6 coating (**Fig. 4(d)**). The cross sectional FE-SEM image of the CZ-6 coating is shown in **Fig. 4 (e)**. An 870 nm thick (Cu, Zr)/a-C thin coating with a smooth and fine grained structure is formed in this coating. Besides, a thin layer of the ZrO_2 layer can be seen on the surface of

the growing coating. As mentioned above, the coatings are partly oxidized due to physical absorption when exposed to air. Here we can conclude that the (Cu, Zr)/a-C thin coatings with higher structural density (compact grain boundaries) and lower defects density (a small number of grain boundary defects and micro cracks) are formed in the coatings with higher Zr contents. The surface roughness of the coatings was obtained from the AFM images and is shown in **Table 2**. The root means square (RMS) roughness of the (Cu, Zr)/a-C thin coatings increased with the increase of the Zr/Cu ratio and reaches to 23 nm for CZ-2 coating and decreases for the coatings with higher Zr/Cu ratios.

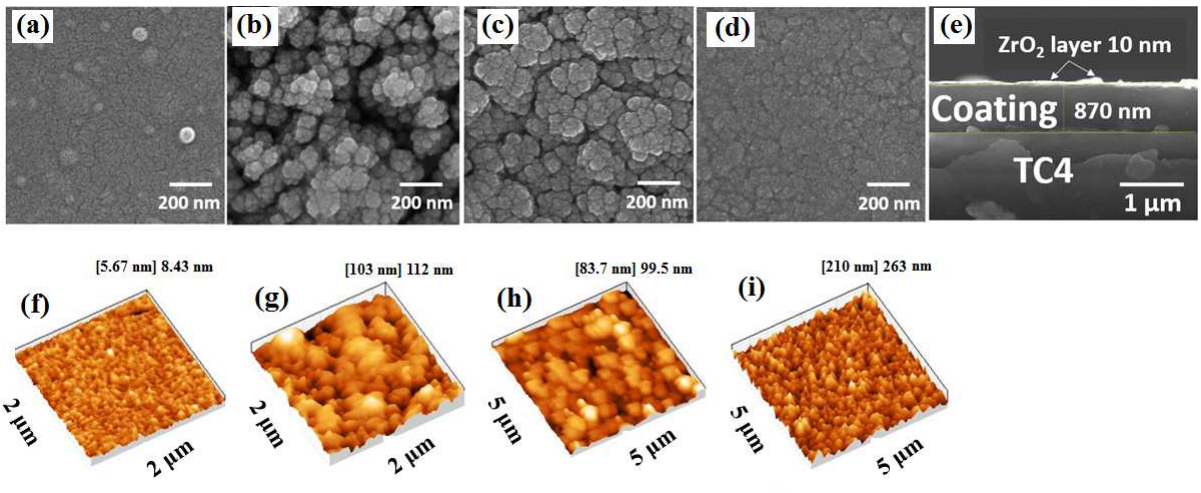

Fig 4. FE-SEM and AFM images of (a) plane view SEM image of CZ-1 coating (b-d) plane view SEM images of CZ-2, CZ-4, and CZ-6 coatings (e) cross-sectional view of CZ-6 coating (f-i) AFM images of CZ-1, CZ-2, CZ-4, and CZ-6 coatings.

The Zr/Cu ratio also affected the internal stress value of the (Cu, Zr)/a-C thin coatings. The internal stress value of the coatings is shown in **Table 2**. All stress values are compressive. It can be seen that the incorporation of a few amounts of Zr affected the internal stress value of (Cu)/a-C thin coating and internal stress value of the (Cu, Zr)/a-C thin coatings increased with increasing Zr/Cu ratio. According to Raman and XPS analysis, (Cu, Zr)/a-C

thin coatings contained a higher fraction of sp^3 bonding and showed diamond-like characteristics. It is well known that a-C coatings with a higher fraction of sp^3 bonding show higher internal stress value, lower adhesion to the metal substrate but better mechanical properties [17,22,50–53]. However, there is a small change in the internal stress value of the coatings with the Zr/Cu ratio, and it might not have any significant impact on the adhesion of the coatings.

The dependence of the mechanical properties of the (Cu, Zr)/a-C thin coatings on the Zr/Cu ratio is shown in **Fig. 5(a)**. The hardness of the (Cu, Zr)/a-C thin coatings remarkably increased with increasing the Zr content. It is well known that Cu is a soft element, and its addition to the a-C matrix does not have any positive impact on the mechanical properties of the (Cu, Zr)/a-C thin coatings [4,7]. In contrast, the incorporation of Zr, which is a hard element, to the a-C matrix, can improve the mechanical properties of the coatings.

Moreover, Zr is a carbide-former element, and the formation of the hard zirconium carbide phase can increase the hardness value of the (Cu, Zr)/a-C thin coatings [26,54]. Besides, as shown above, (Cu, Zr)/a-C, the thin coatings with a higher Zr/Cu ratio have higher internal stress values and contain a higher proportion of the sp^3 bonds and increased the diamond domain size. This can be another piece of evidence for better mechanical properties of (Cu, Zr)/a-C thin coatings containing higher Zr content. The H^3/E^2 ratio, which is known as the plasticity index, is an essential parameter determining the tribological properties and wear resistance of the thin coatings [54,55]. The variation of the H^3/E^2 ratio with the Zr/Cu ratio is plotted in **Fig. 5(b)**. It can be seen that the plasticity index of the CZ-2, 3 coatings with lower Zr/Cu, takes higher values than that of the CZ-1 coating without Zr. However, the plasticity index of the (Cu, Zr)/a-C thin coatings containing higher Zr/Cu decreased, even down to that of CZ-1 coating with no Zr.

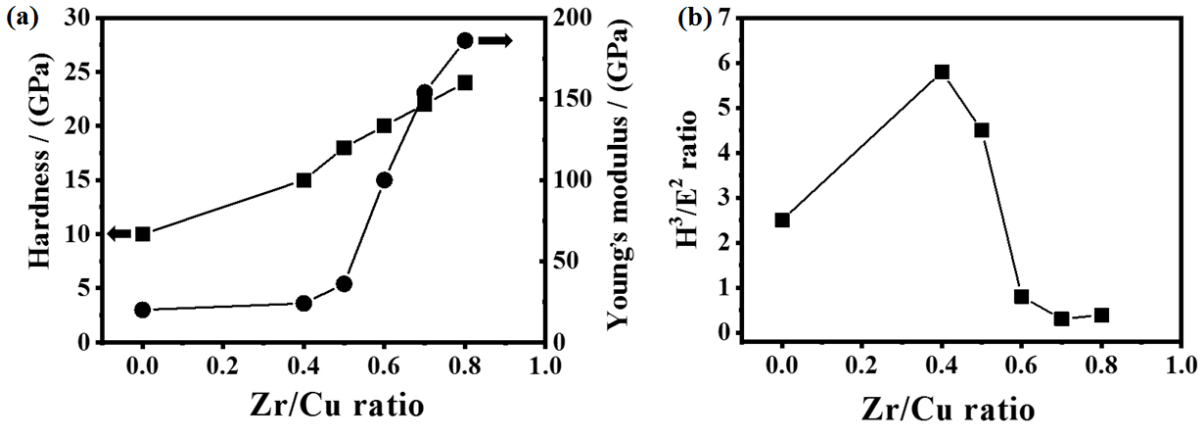

Fig. 5. Influence of Zr/Cu ratio on (a) plastic hardness and Young's modulus and (b) H^3/E^2 ratio of the coatings.

The bio-corrosion resistance of the TC4 alloy samples, coated by Cu/a-C (CZ-1) and various (Cu, Zr)/a-C (CZ-2 to CZ-6) thin coatings, was studied by EIS and polarization analyses in SBF solution for various times. The Nyquist and Bode diagrams of the prepared samples after 5, 24, 48, and 168 h exposure to the SBF solution was displayed in **Figs. 6** and **7**. It can be observed that the blank sample showed the lowest diameter of semi-circles and impedance modulus values at low frequencies in Bode plots. For the samples coated by Cu/a-C (CZ-1), the diameter of semi-circles and impedance at low frequencies (0.01 Hz) clearly increased after 48 h. As time elapsed, these values decreased because of the occurrence of electrolyte diffusion through the coating defects [56,57]. Furthermore, the neat TC4 alloy only showed one relaxation time, while two relaxation times were detected for the CZ-1 in all of the immersion times. This could be assigned to the presence of a barrier coating originated from copper on the surface [58–60].

In the case of the various (Cu, Zr)/a-C thin coatings (CZ-2 to CZ-6), the diameter of the semi-circles and impedance values (0.01 Hz) showed an ascending trend and reached a maximum value after 168 h immersion time. The ascending trend of the semi-circle diameter for these samples (CZ-2 to CZ-6) implies that the presence of Zr activates the construction of

a protective barrier layer. [61,62]. Additionally, a new time constant appeared for these samples, confirming the passive coating formation by zirconium. The protection performance of the coatings clearly surges with the increment of the zirconium. In other words, the semi-circle was the largest for CZ-6, indicating its superior protection performance for TC4 alloy. The phase angle at high-frequency values showed similar trend like the impedance values. Accordingly, it is rational to deduce that the massive difference of the protection ability from samples 1 to 6 (prepared coatings) is related to the disparate layer design that is scrupulously linked to the content of Zr as well as the synergism between the Zr and Cu. With the increased Zr content, the negative phase angle values are illustrated from samples 1 to 6 at all exposure periods. The more negative phase angle values of CZ-6 reflects the best corrosion protection for this sample [63–65].

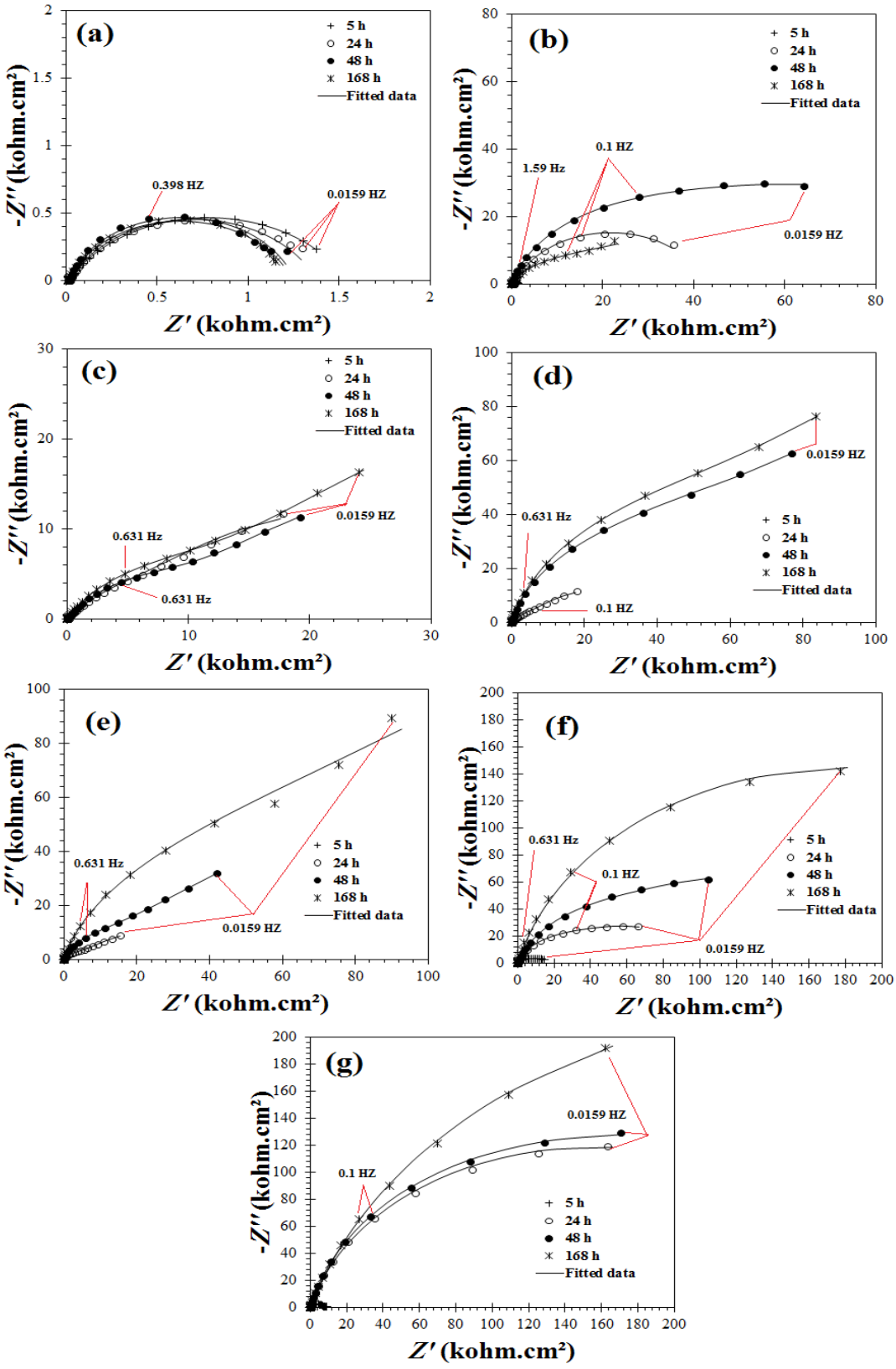

Fig. 6. Nyquist plots of (a) blank, (b) CZ-1, (c) CZ-2, (d) CZ-3, CZ-4, CZ-5 and (e) CZ-6 immersed in the SBF solution; solid lines and marker points are attributed to the fitted and experimental data, respectively.

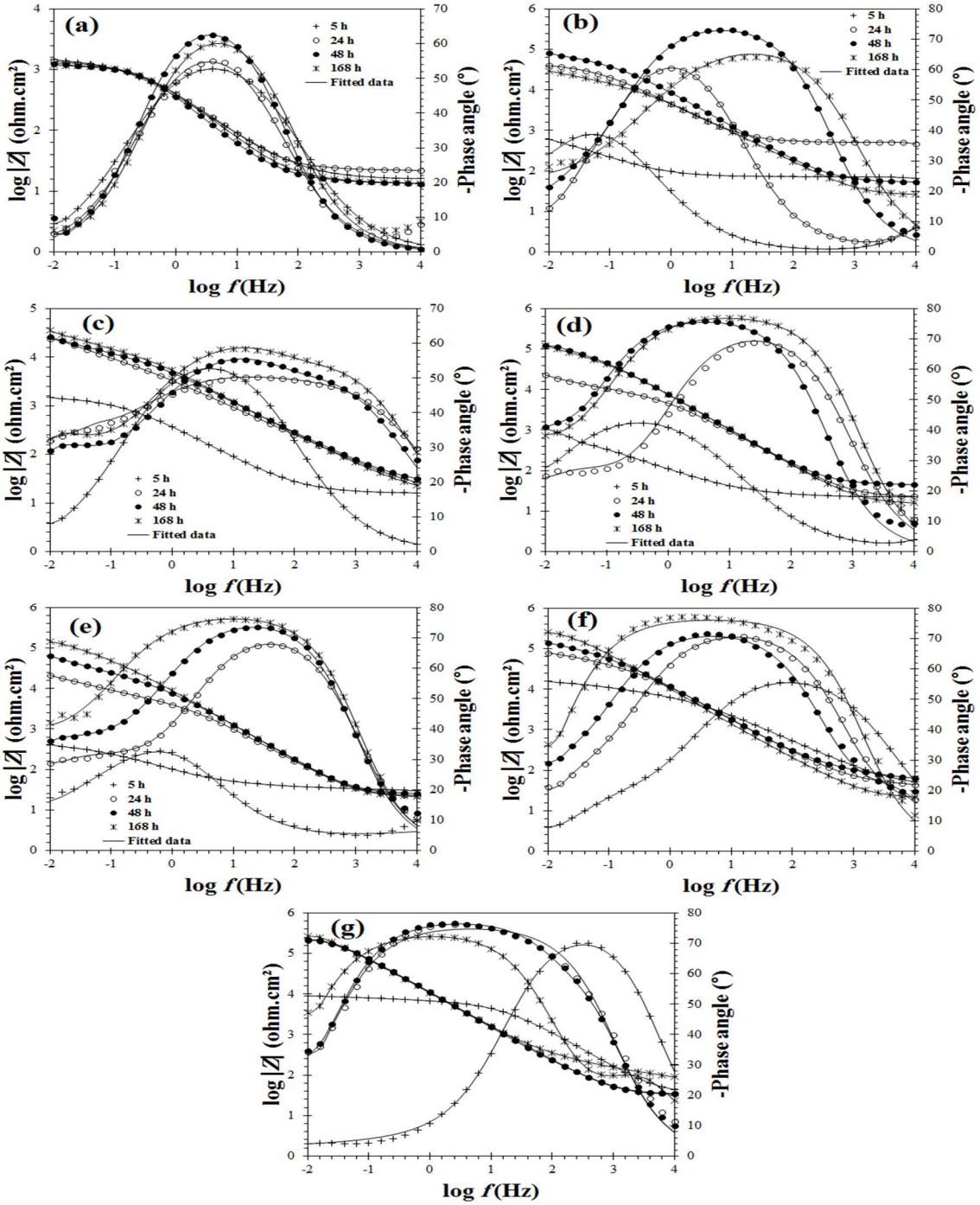

Fig. 7. Bode plots of the (a) blank, (b) CZ-1, (c) CZ-2, (d) CZ-3, CZ-4, CZ-5 and (e) CZ-6 immersed in the SBF solution; solid lines and marker points are attributed to the fitted and experimental data, respectively

Three equivalent circuits were exploited to simulate the EIS data, as shown in **Fig. 8**. The first pattern (**Fig.8a**) has been exerted to qualify the corrosion process of the TC4 alloy samples exposed to the SBF solution. The reason for choosing such a model is that there is an

only one-capacitive loop in the Nyquist and Bode-phase plots of this sample, indicating that the occurrence of corrosion reactions on this sample is under charge-transfer mechanism control. The second and third models were employed to parse the electrochemical action of TC4 alloy samples coated by Cu/a-C (CZ-1) and various (Cu, Zr)/a-C coatings (CZ-2 to CZ-6), respectively. The reason for choosing these models is that there is two or three capacitive loops in the EIS plots of these samples, revealing that the presence of protective films on the surface. In the third model, the relaxation times at low-frequency, middle frequency, and high-frequency can be associated with the double layer, an oxide layer (due to the presence of zirconium oxide), and film resistance, respectively. In these models, the R_s indicates the SBF solution resistance, R_{ct}, R_f, and R_{ox} are the charge transfer resistance, the coating resistance, and the oxide layer resistance, respectively. CPE_{dl}, CPE_{ox}, and CPE_f are the constant phase elements displaying the non-ideal capacitance of the double layer, oxide layer, and protective coating, respectively. The fitting results are presented in **Table 4**. In this table, n and Y represent the exponent and admittance of the constant phase element, respectively.

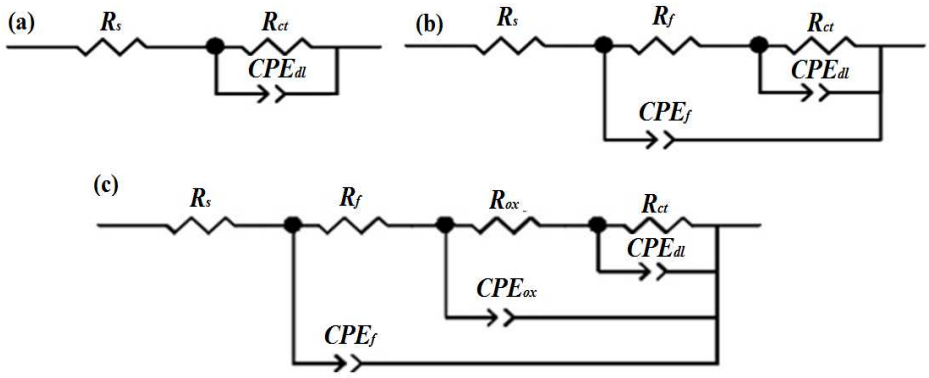

Fig. 8. Electrical equivalent circuits for simulating the EIS spectra with (a) one (b) two and (c) three relaxation times.

Table 4. Variation of EIS electrochemical parameters of samples immersed in the SBF solution after 168 h.

Sample	Time (h)	R_{ct} [a] (kΩ.cm^2)	$Y_{0,dl}$ [b] (μs^n.Ω^{-1}.cm^{-2})	n_{dl} [c]	R_{ox} [a] (kΩ.cm^2)	$Y_{0,ox}$ [b] (μs^n.Ω^{-1}.cm^{-2})	n_{ox} [c]	R_f [a] (kΩ.cm^2)	$Y_{0,f}$ [b] (μs^n.Ω^{-1}.cm^{-2})	n_f [c]
Blank (without coating)	**5**	1.53	517.3	0.70	-	-	-	-	-	-
	24	1.36	569	0.75	-	-	-	-	-	-
	48	1.24	575.6	0.79	-	-	-	-	-	-
	168	1.23	576.8	0.82	-	-	-	-	-	-
CZ-1	**5**	1.16	505.1	0.66	-	-	-	0.036	4.8	0.98
	24	42.48	52.3	0.79	-	-	-	0.167	3.5	0.98
	48	53.51	34.8	0.71	-	-	-	5.36	2.3	0.78
	168	55.51	11.2	0.69	-	-	-	56.08	1.5	0.85
CZ-2	**5**	1.19	485	0.98	-	-	-	0.395	52.7	0.69
	24	25.47	213	0.82	19.77	31.3	0.53	0.794	52.5	0.63
	48	44.52	276.5	0.70	1.432	6.3	0.83	1.53	46.9	0.66
	168	88.18	180.4	0.66	18.07	4.4	0.77	1.02	37.1	0.69
CZ-3	**5**	1.24	304	0.97	-	-	-	0.354	13.6	0.98
	24	1.57	277	0.98	30.90	24.8	0.61	10.38	32.9	0.83
	48	226	164.7	0.81	37.54	24.5	0.90	51.35	28.1	0.85
	168	339.20	101.1	0.77	48.99	23.6	0.95	55.36	25.9	0.87
CZ-4	**5**	1.87	295	0.77	-	-	-	0.361	32.1	0.62
	24	5.63	241.6	0.98	33.65	17.9	0.53	12.32	27.5	0.83
	48	245.70	78.9	0.72	45.20	14.1	0.69	71.39	14.1	0.86
	168	386.23	59.1	0.74	52.17	12.1	0.69	123.41	9.7	0.85
CZ-5	**5**	12.65	24.2	0.55	-	-	-	2.57	4.5	0.87
	24	56.01	76.5	0.69	46.26	4.2	0.81	2.032	3.7	0.85
	48	200	65.6	0.81	113.30	2.1	0.82	7.30	3.1	0.83
	168	221.65	5.1	0.80	387.70	1.8	0.84	95.63	2.2	0.78
CZ-6	**5**	15.19	16.7	0.95	-	-	-	4.33	4.3	0.97
	24	48.33	10.2	0.95	47.23	3.5	0.84	10.36	4.1	0.98
	48	269	2.7	0.98	299.20	1.9	0.86	152.69	1.9	0.86
	168	274.27	1.3	0.95	450.59	1.6	0.67	363.95	1.4	0.85

a. The standard deviation range is between 1.2 and 16.7%.
b. The standard deviation range is between 1.7 and 7.6%.
c. The standard deviation range is between 0.2 and 0.9%.

It is accepted that the protective properties of a coating can be presupposed from the summation of resistances (R_p, polarization resistance) [66–68]. These values for the prepared panels after various periods are summarized in **Fig. 9**. The lowest R_p was observed for the blank sample. The R_p decrements were based on the electrolyte diffusion through the defects, and holes exist in the coating [69,70]. After 168 h immersion, the R_p of the blank sample in the SBF solution reached the lowest value of 1.2 kΩ.cm^2, while the R_p increased to 40.2 kΩ.cm^2 with the addition of copper. It is vivid that the R_p values for the panels including Zr

and Cu, increased with time up to 168 h while the sample containing only Cu (CZ-1) showed R_p increment up to 48 h and then a reduction occurred. It can be subsumed that all of the (Cu, Zr)/a-C thin coatings demonstrated protection behaviors, due to the synergism between the Zr and Cu. About (Cu, Zr)/a-C thin coatings, the R_p of the CZ-6 was the biggest with a value of 990 kΩ.cm^2, verifying that the CZ-6 could provide the excellent and exceptional protection for TC4. This might be due to the presence of more protection agents (Zr and Cu) on the cathodic regions and the formation of a more uniform and compact barrier layer, which can be confirmed by **Fig. 8**. This figure includes useful models that can be used to illustrate the difference between the various coatings. According to **Fig. 8**, a relaxation-time is added by adding each protective agent (Cu or Zr) to the system. However, some studies have shown that change in microstructures and phase constituents of titanium and titanium matrix composites could have a significant impact on their corrosion resistance and that ultrafine particles of metallic materials could significantly decrease fluctuation of the passive film and strengthen its stability [71,72]. This means that the dissolution of the titanium matrix takes place almost simultaneously as the establishment of the TiO_2 film in the passivation process. Previous investigations [71,72] reveal that the presence of substantial Cl^- outcomes in the corrosion of titanium to form $[TiCl_6]^{2-}$ complex and that these chlorocomplex benefits for the passive performance of titanium matrix materials. Therefore, it can be said that the protection ability and stability of the passive film on the surface of the CZ-6 sample is better than those of other samples. The results also represent that the R_f value of CZ-6 at the end of immersion is considerably higher than that of other samples. Usually, a higher amount of R_f means better corrosion protection of this sample [73,74].

The homogeneity of the thin film formed on the TC4 alloy surface was evidenced by higher 'n_{dl}' value as a heterogeneity index for the CZ-6 in comparison with the lower value of 'n_{dl}' for the other samples [75,76].

The evolution of the admittance values (*Y* from **Table 4**) of the samples represents that the blank sample (TC4 alloy without coating) had the highest values among the examined specimens in all of the immersion times. The admittance of the CZ-6 sample is much lower than that for the other coated specimens in all of the immersion times. The decrease in the admittance values could be linked to the increase in the electrical double layer thickness or the formation of a protective film. This result clearly shows that the corrosion of TC4 alloy in the SBF solution is limited by the application of the coating.

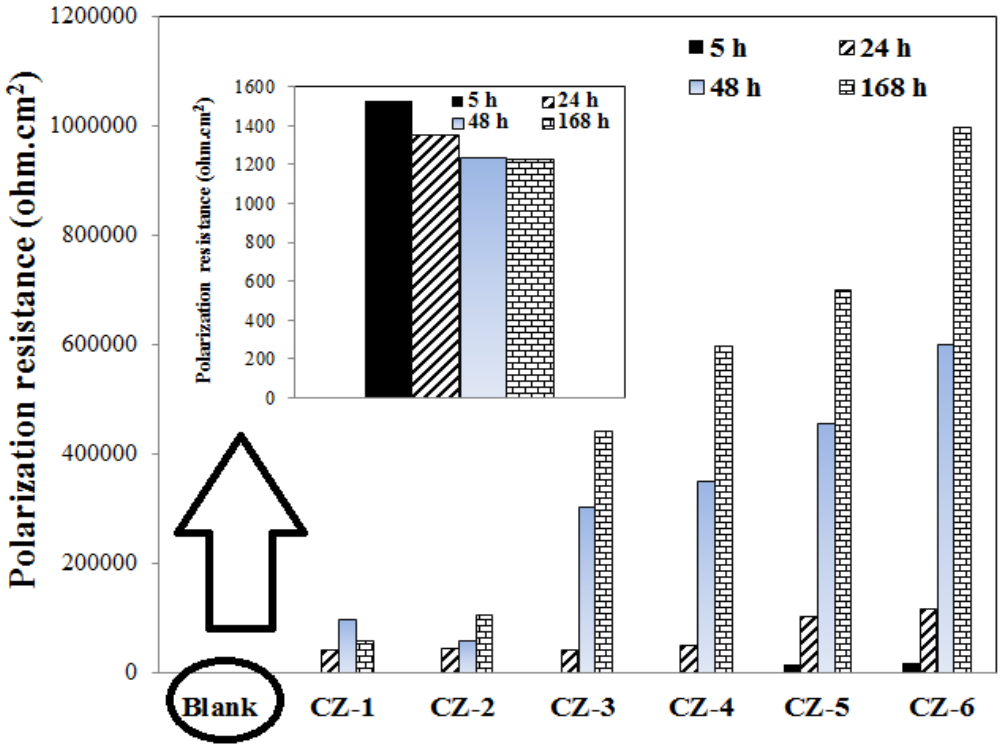

Fig. 9. Polarization resistance values of prepared samples in various immersion time.

To more profoundly explore the mechanism of the corrosion protection behavior of the coated samples (CZ-1 and CZ-6), a polarization test was performed, and the associated curves are depicted in **Fig. 10**. As can be seen, the polarization curves of the coated samples shifted to the negative values compared to the blank sample. This result reveals the cathodic behavior of the coated samples due to the presence of Cu and Zr in the structure, leading to

the oxygen reduction reaction limitation. Results also indicated a decrease in the corrosion current density of the coated samples compared to the blank sample. This reveals the protection ability of the CZ-1 and CZ-6 samples.

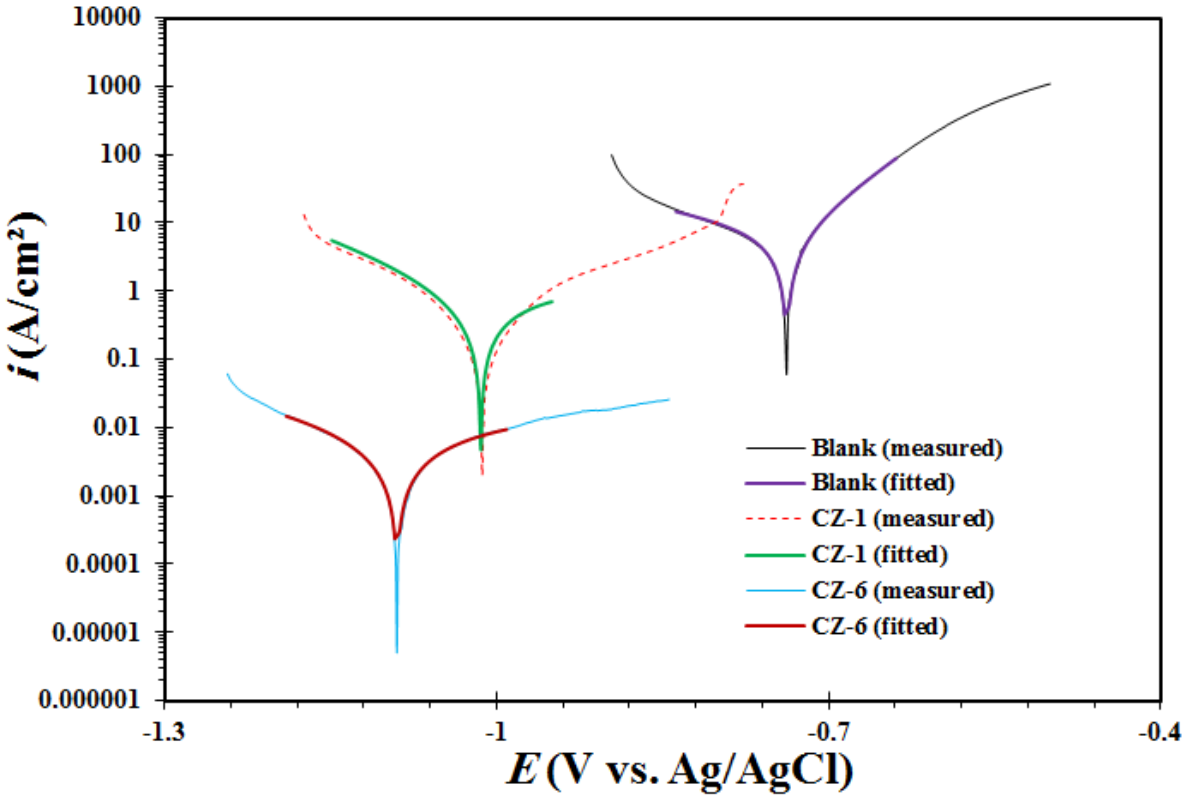

Fig. 10. Polarization curves of the prepared samples immersed in SBF solution after 168 h

Corrosion current density (i_{corr}), corrosion potential (E_{corr}), anodic (β_a) and cathodic (β_c) slopes were derived from Wagner-Traud model fitting [77] and reported in **Table 5**. The polarization resistance could be also calculated by using the equation (1) [78] and the corresponding results are listed in **Table 5**.

$$R_P = \frac{\beta_a|\beta_c|}{2.303(\beta_a + \beta_c)i_{corr}} \qquad (1)$$

From **Table 5**, the corrosion current density of the cathodic and anodic slopes reduced. This indicates a significant change in the mechanisms of the anodic and cathodic reactions. After

168 h, the CZ-6 sample has the lowest i_{corr} value among all other samples, which is around 0.061 μA/cm^2. The reduction of about two orders of magnitude of the corrosion current density of the CZ-6 compared to the CZ-1 confirmed the synergism role of the Cu and Zr to limit the corrosion development. This ability is mainly provided by the formation of the protective film on the cathodic areas. The result showed a higher R_p value of CZ-6 sample in the SBF solution than the rest of the samples. All of the results corroborate each other and reveal the effectiveness of the CZ-6 sample in long immersion times.

Table 5: Electrochemical parameters derived from Tafel extrapolation fitting plots of the prepared samples immersed in SBF solution after 168 h

Sample	E_{corr} ***vs.*** **Ag/Agcl (mV)**	i_{corr} **(A/cm^2)**	β_a **(V/dec)**	$-\beta_c$ **(V/dec)**	R_p **(kΩ/cm^2)**
Blank	-760.9 ± 11.4	(6.7±0.5)×10^{-6}	0.037 ± 0.05	0.161± 0.03	1.9±0.2
CZ-1	-1015 ± 18.3	(1.2±0.1)×10^{-6}	0.812 ± 0.07	0.312 ± 0.09	108.7±1.1
CZ-6	-1089 ± 14.5	(6.1±0.05)×10^{-8}	0.512 ± 0.15	0.217 ± 0.08	1084.7±0.9

a. The standard deviation range is between 1.2 and 6.9%.

As discussed above, both Cu/a-C and (Cu, Zr)/a-C thin coatings provide TC4 substrate with high corrosion resistance. However, the bio-corrosion protection properties of the (Cu, Zr)/a-C thin coatings are much higher than the Cu/a-C thin coating. This shows the positive effect of the Zr addition on the bio-corrosion resistance of Cu/a-C thin coating. Moreover, the corrosion resistance performance of (Cu, Zr)/a-C thin coatings is notably improved with increasing the Zr/Cu ratio. As shown above, the (Cu, Zr)/a-C thin coatings possess lower structural density and higher defects density compare to the Cu/a-C thin coating (**Fig. 4**). The defective structure, which is containing pinholes, micro-cracks, and open grain boundaries,

provides a direct penetration path for corrosive entities towards the metal substrate and deteriorates its corrosion resistance. However, it seems that the defective structure and higher roughness of the (Cu, Zr)/a-C thin coatings do not have considerable impact on the bio-corrosion resistance and the chemical composition of the coatings and presence of Zr, is the dominant factor, improving the bio-corrosion resistance of the (Cu, Zr)/a-C thin coatings. It has been shown that ZrO_2 is a high corrosion resistance compound [79–82]. Accordingly, it can be concluded that the formation of zirconia as the corrosion product can act as a protective compound against corrosive media and improves the bio-corrosion resistance of the (Cu, Zr)/a-C thin coatings compared to that of Cu/a-C thin coating. The bio-corrosion resistance of (Cu, Zr)/a-C thin coatings increased with the increasing the Zr/Cu ratio. The higher corrosion resistance of the coatings with a higher Zr/Cu ratio can be explained by several facts. Based on the Raman analysis of the samples (**Fig. 1**), an amorphous-like structure is formed in (Cu, Zr)/a-C thin coatings with higher Zr/Cu ratios. It has been demonstrated that the amorphous materials show high corrosion resistance in various solutions [7,83,84]. This resistance is ascribed to their chemical homogeneity and absence of structural defects (dislocations and grain boundaries) [7,83,84]. The structural homogeneity leads to the formation of a uniform passive layer, which can insulate the metal substrate from the aggressive media [85]. Moreover, as discussed above, the formation of the ZrO_2, as a high corrosion resistance compound and its passive property, can be another reason for the superior anti-corrosion properties of the coatings with a higher Zr/Cu ratio [79–82]. The final reason might be the morphology of the coating. As shown in **Fig. 4**, (Cu, Zr)/a-C thin coatings with lower Zr/Cu ratios (CZ-2, 4) show defective structure with open grain boundaries, which make the open paths for the aggressive environment to penetrate the coating and deteriorate its corrosion-resistant. In contrast, the (Cu, Zr)/a-C thin coating with a higher Zr/Cu ratio (CZ-6) shows a homogeneous structure with lower defects density. The

homogeneous structure prevents penetration of the corrosive environment and improves the corrosion resistance of (Cu, Zr)/a-C thin coating with a higher Zr/Cu ratio (CZ-6).

Conclusions

The synergistic effects of Cu and Zr on microstructure, mechanical and bio-corrosion performance of the resulting thin coatings were studied and discussed using Raman, XPS, hardness, plasticity index, and electrochemical methods and the following main conclusions were obtained:

- The Raman and XPS analysis of the coatings revealed that the (Cu, Zr)/a-C thin coatings with low Zr content contain a higher proportion of sp^3 bonded carbons and bigger diamond-like domain size. In contrast, the presence of the higher Zr content (Zr/Cu=0.5-0.8) breaks the long-range order of the graphite structure.
- The mechanical and bio-corrosion properties of the coatings show a significant dependence on Zr and Cu content.
- It is concluded that (Cu, Zr)/a-C thin coatings with higher structural density and lower defects density are formed in the coatings with higher Zr contents.
- The hardness of (Cu, Zr)/a-C thin coatings increased with the increasing Zr/Cu ratio. (Cu, Zr)/a-C thin coatings with lower Zr/Cu ratios showed a higher plasticity index (H3/E2).
- Both Cu/a-C and (Cu, Zr)/a-C thin coatings revealed excellent bio-corrosion resistance to the TC4 substrate. However, (Cu, Zr)/a-C thin coatings showed superior bio-corrosion resistance, and Zr content of the coatings played a significant role.
- The results of the present study confirmed that a right combination of high hardness and superior bio-corrosion resistance of (Cu, Zr)/a-C thin coatings could be obtained with co-doping of Cu and Zr. It is speculated that such co-doped a-C coatings can be

promising candidates for biomedical applications. For instance, such (Cu, Zr)/a-C thin coatings with high hardness and excellent bio-corrosion resistance can be used as protective coatings on the surface of medical implants.

References

[1] N. Jalali, F. Mokhtarzadeh, A. Asgari, A. Zamanian, K. Verma, M. Mozafari, Improving cellular response of titanium surface through electrochemical anodization for biomedical applications: A critical review, Trends Biomater. Artif. Organs., 29 (2015), pp. 86–91.

[2] T. Ye, L. Song, Y. Liang, M. Quan, J. He, J. Lin, Precipitation behavior of ωo phase and texture evolution of a forged Ti-45Al-8.5Nb-(W, B, Y) alloy during creep, Mater. Charact., 136 (2018), pp.41–51.

[3] A. Nemati, M. Saghafi, S. Khamseh, E. Alibakhshi, P. Zarrintaj, M.R. Saeb, Magnetron-sputtered TixNythin films applied on titanium-based alloys for biomedical applications: Composition-microstructure-property relationships, Surf. Coat. Technol. 349 (2018), pp. 251–259.

[4] Y. Cheng, Y.F. Zheng, Formation of TiN films on biomedical NiTi shape memory alloy by PIIID, Mater. Sci. Eng. A., 434 (2006), pp. 99–104.

[5] J. Probst, U. Gbureck, R. Thull, Binary nitride and oxynitride PVD coatings on titanium for biomedical applications, Surf. Coat. Technol., 148 (2001), pp. 226–233.

[6] H.J. Brading, P.H. Morton, T. Bell, L.G. Earwalsûer, The structure and composition of plasma nitrided coatings on titanium, Nucl. Instru. Meth. Phys. Res. Sect. B Beam Interact. with Mater. Atoms., 66 (1992), pp. 230–236.

[7] S. Khamseh, E. Alibakhshi, M. Mahdavian, M.R. Saeb, H. Vahabi, J.-S. Lecomte, P. Laheurte, High-performance hybrid coatings based on diamond-like carbon and copper for carbon steel protection, Diam. Relat. Mater., 80 (2017) pp. 84–92.

[8] S. Khamseh, E. Alibakhshi, M. Mahdavian, M.R. Saeb, H. Vahabi, N. Kokanyan, P. Laheurte, Magnetron-sputtered copper/diamond-like composite thin films with super anti-corrosion properties, Surf. Coat. Technol., 333 (2018,) pp. 148–157.

[9] T.F. Zhang, Q.Y. Deng, B. Liu, B.J. Wu, F.J. Jing, Y.X. Leng, N. Huang, Wear and corrosion properties of diamond like carbon (DLC) coating on stainless steel, CoCrMo and Ti6Al4V substrates, Surf. Coat. Technol., 273 (2015), pp. 12–19.

[10] R. Hatada, S. Flege, A. Bobrich, W. Ensinger, K. Baba, Surface modification and corrosion properties of implanted and DLC coated stainless steel by plasma based ion implantation and deposition, Surf. Coat. Technol., 256 (2014) pp. 23–29.

[11] M. Azzi, P. Amirault, M. Paquette, J.E. Klemberg-Sapieha, L. Martinu, Corrosion performance and mechanical stability of 316L/DLC coating system: Role of interlayers, Surf. Coat. Technol., 204 (2010), pp. 3986–3994.

[12] J. Robertson, Diamond-like amorphous carbon, Mater. Sci. Eng. R., 37 (2002), pp. 129–281.

[13] L. Sun, P. Guo, X. Li, A. Wang, Comparative study on structure and wetting properties of diamond-like carbon films by W and Cu doping, Diam. Relat. Mater., 73 (2017), pp. 278–284.

[14] N.W. Khun, P.M. Lee, W.Q. Toh, E. Liu, Tribological behavior of nickel-doped diamond-like carbon thin films prepared on silicon substrates via magnetron sputtering deposition, Tribol. Trans., 59 (2016), pp. 845–855.

[15] F. Cemin, L.T. Bim, L.M. Leidens, M. Morales, I.J.R. Baumvol, F. Alvarez, C.A. Figueroa, Identification of the chemical bonding prompting adhesion of a-C:H thin films on ferrous alloy intermediated by a SiCx:H buffer layer, ACS Appl. Mater. Interfaces., 7 (2015), pp. 15909–15917.

[16] J.S. Chen, S.P. Lau, Z. Sun, G.Y. Chen, Y.J. Li, B.K. Tay, J.W. Chai, Metal-containing amorphous carbon films for hydrophobic application, Thin Solid Films., 398–399 (2001), pp. 110–115.

[17] M.Y. Ming, X. Jiang, D.G. Piliptsou, Y. Zhuang, A. V. Rogachev, A.S. Rudenkov, A.

Balmakou, Chromium-modified a-C films with advanced structural, mechanical and corrosive-resistant characteristics, Appl. Surf. Sci., 379 (2016), pp. 424–432.

[18] L.Y. Ostrovskaya, V.M. Perevertailo, L.A. Matveeva, P. Milani, V.G. Ralchenko, E.M. Shpilevsky, Characterization of different carbon nanomaterials promising for biomedical and sensor applications by the wetting method, Powder Metall. Met. Ceram., 42 (2003) pp. 1–8.

[19] Y.H. Chan, C.F. Huang, K.L. Ou, P.W. Peng, Mechanical properties and antibacterial activity of copper doped diamond-like carbon films, Surf. Coat. Technol., 206 (2011), pp. 1037–1040.

[20] Y. Liu, P. Guo, X. He, L. Li, A. Wang, H. Li, Developing transparent copper-doped diamond-like carbon films for marine antifouling applications, Diam. Relat. Mater., 69 (2016), pp. 144–151.

[21] M.Y. Tsai, M.S. Huang, L.K. Chen, Y.D. Shen, M.H. Lin, Y.C. Chiang, K.L. Ou, S.F. Ou, Surface properties of copper-incorporated diamond-like carbon films deposited by hybrid magnetron sputtering, Ceram. Int., 39 (2013), pp. 8335–8340.

[22] N. Dwivedi, S. Kumar, H.K. Malik, C. Sreekumar, S. Dayal, C.M.S. Rauthan, O.S. Panwar, Investigation of properties of Cu containing DLC films produced by PECVD process, J. Phys. Chem. Solids., 73 (2012), pp. 308–316.

[23] P. Kubasiewicz-Ross, M. Dominiak, T. Gedrange, U. Botzenhart, Zirconium: The material of the future in modern implantology, Adv. Clin. Exp. Med., 26 (2017), pp. 533–537.

[24] M. Mozafari, E. Salahinejad, V. Shabafrooz, M. Yazdimamaghani, D. Vashaee, L. Tayebi, Multilayer bioactive glass/zirconium titanate thin films in bone tissue engineering and regenerative dentistry, Int. J. Nanomedicine., 8 (2013), pp. 1665–1672.

[25] Q.N. Meng, M. Wen, F. Mao, N. Nedfors, U. Jansson, W.T. Zheng, Deposition and characterization of reactive magnetron sputtered zirconium carbide films, Surf. Coat. Technol., 232 (2013), pp. 876–883.

[26] W.Q. Bai, Y.J. Xie, L.L. Li, X.L. Wang, C.D. Gu, J.P. Tu, Tribological and corrosion behaviors of Zr-doped graphite-like carbon nanostructured coatings on Ti6Al4V alloy, Surf. Coat. Technol. 320 (2017) pp. 235–239.

[27] T. Vitu, A. Escudeiro, T. Polcar, A. Cavaleiro, Sliding properties of Zr-DLC coatings: The effect of tribolayer formation, Surf. Coat, Technol., 258 (2014), pp. 734–745.

[28] S. Zhou, L. Wang, S.C. Wang, Q. Xue, Comparative study of simplex doped nc-WC / a-C and duplex doped nc-WC / a-C (Al) nanocomposite coatings, Appl. Surf. Sci., 257 (2011), pp. 6971–6979.

[29] Z. Zhang, H. Zhou, D. Guo, H. Gao, R. Kang, Optical characterization of hydrogen-free CeO_2 doped DLC films deposited by unbalanced magnetron sputtering, Appl. Surf. Sci., 255 (2008), pp. 2655–2659.

[30] J. Jao, S. Han, L. Chang, C. Chang, Y. Liu, H.C. Shih, Bias voltage effect on the structure and property of chromium copper – diamond-like carbon multilayer films fabricated by cathodic arc plasma, Appl. Surf. Sci., 256 (2010), pp. 7490–7495.

[31] B. Window, N. Savvides, Unbalanced dc magnetrons as sources of high ion fluxes, J. Vac. Sci. Technol. A., 4 (1986) pp. 453–456.

[32] X. Liu, J. Yang, J. Hao, J. Zheng, Q. Gong, W. Liu, Microstructure , mechanical and tribological properties of Si and Al co-doped hydrogenated amorphous carbon fi lms deposited at various bias voltages, Surf. Coat. Technol., 206 (2012), p. 4119–4125.

[33] X. Liu, J. Hao, J. Yang, J. Zheng, Y. Liang, W. Liu, X. Liu, J. Hao, J. Yang, J. Zheng, Y. Liang, Preparation of superior lubricious amorphous carbon films co-doped by silicon and aluminum Preparation of superior lubricious amorphous carbon films co-

doped by silicon and aluminum, J. Appl. Phys., 110 (2011) p. 053507.

[34] X. Li, P. Guo, L. Sun, X. Zuo, D. Zhang, P. Ke, A. Wang, Ti / Al co-doping induced residual stress reduction and bond structure evolution of amorphous carbon fi lms : An experimental and ab initio study, Carbon., 111 (2017), pp. 467–475.

[35] W. Wu, Z. Zhu, J. Min, J. Zhang, N. Qian, M. Jiang, Adhesion behavior of diamond-like carbon films with F and Si co-doping prepared by radio frequency reactive magnetron sputtering, Thin Solid Films., 622 (2017), pp. 89–94.

[36] X. Liu, Y. Lin, J. Xiang, J. Hao, X. Wan, Dual-doped (Si-Ag) graphite-like carbon coatings with ultra-low friction and high antibacterial activity prepared by magnetron sputtering deposition, Diam. Relat. Mater., 86 (2018), pp. 47–53.

[37] L. Sun, P. Guo, P. Ke, X. Li, A. Wang, Synergistic effect of Cu / Cr co-doping on the wettability and mechanical properties of diamond-like carbon fi lms, Diam. Relat. Mater., 68 (2016), pp. 1–9.

[38] M.R. Derakhshandeh, M.J. Eshraghi, M. Javaheri, S. Khamseh, M.G. Sari, P. Zarrintaj, M.R. Saeb, M. Mozafari, Diamond-like carbon-deposited films: a new class of biocorrosion protective coatings, Surf. Innov., 6 (2018), pp. 266–276.

[39] M.R. Derakhshandeh, M.J. Eshraghi, M.M. Hadavi, M. Javaheri, S. Khamseh, M.G. Sari, P. Zarrintaj, M.R. Saeb, M. Mozafari, Diamond-like carbon thin films prepared by pulsed-DC PE-CVD for biomedical applications, Surf. Innov., 6 (2018), pp. 167–175.

[40] R. Bayon, A. Igartua, J.J. Gonzalez, U. Ruiz De Gopegui, Influence of the carbon content on the corrosion and tribocorrosion performance of Ti-DLC coatings for biomedical alloys, Tribol. Int., 88 (2015), pp. 115–125.

[41] P.C.T. Ha, D.R. McKenzie, M.M.M. Bilek, S.C.H. Kwok, P.K. Chu, B.K. Tay, Raman spectroscopy study of DLC films prepared by RF plasma and filtered cathodic arc,

Surf. Coat.Technol., 201 (2007), pp. 6734–6736.

[42] J. Cui, L. Qiang, B. Zhang, X. Ling, T. Yang, J. Zhang, Mechanical and tribological properties of Ti-DLC films with different Ti content by magnetron sputtering technique, Appl. Surf. Sci., 258 (2012), pp. 5025–5030.

[43] H. Hasan, V. Abdelsayed, A. Kheder, K. AbouZeid, J. Terner, M. El-Shall, S. Al-Resayes, A. El-Azhary, Microwave synthesis of graphene sheets supporting metal nanocrystals in aqueous and organic media, J. Mater. Sci., 19 (2009), pp. 3832–3837.

[44] N. Hellgren, M. Johansson, E. Broitman, L. Hultman, J.-E. Sundgren, Role of nitrogen in the formation of hard and elastic CNx thin films by reactive magnetron sputtering, Phys. Rev. B., 59 (1999), pp. 5162–5169.

[45] L. Ji, H. Li, F. Zhao, J. Chen, H. Zhou, Microstructure and mechanical properties of Mo/DLC nanocomposite films, Diam. Relat. Mater., 17 (2008), pp. 1949–1954.

[46] S. Wei, W.P. Kang, J.L. Davidson, J.H. Huang, Aligned carbon nanotubes fabricated by thermal CVD at atmospheric pressure using Co as catalyst with NH_3 as reactive gas, Diam. Relat. Mater., 15 (2006), pp. 1828–1833.

[47] M. Andersson, S. Urbonaite, E. Lewin, U. Jansson, Magnetron sputtering of Zr – Si – C thin films, Thin Solid Films., 520 (2012), pp. 6375–6381.

[48] W. Dai, H. Zheng, G. Wu, A. Wang, Effect of bias voltage on growth property of Cr-DLC film prepared by linear ion beam deposition technique, Vacuum., 85 (2010), PP. 231–235.

[49] D. Choudhury, J. Lackner, R.A. Fleming, J. Goss, J. Chen, M. Zou, Diamond-like carbon coatings with zirconium-containing interlayers for orthopedic implants, J. Mech. Behav. Biomed. Mater., 68 (2017), pp. 51–61.

[50] J.H. Choi, A. H.S., S.C. Lee, K.R. Lee, Stress reduction behavior in metal-incorporated amorphous carbon films : first-principles approach, J. Phys. Conf. Ser.,

29 (2006), pp. 155–158.

[51] E. Broitman, W.T. Zheng, H. Sjöström, I. Ivanov, J.E. Greene, J.E. Sundgren, Stress development during deposition of CNx thin films, Appl. Phys. Lett., 72 (1998), pp. 2532–2534.

[52] P. Couvrat, M. Denis, M. Langer, S. Mitura, P. Niedzielski, J. Marciniak, The corrosion tests of amorphous carbon coatings deposited by r.f. dense plasma onto steel with different chromium contents, Diam. Relat. Mater., 4 (1995), pp. 1251–1254.

[53] D.G. Liu, J.P. Tu, R. Chen, C.D. Gu, Microstructure, corrosion resistance and biocompatibility of titanium incorporated amorphous carbon nitride films, Surf. Coat. Technol., 206 (2011), pp. 165–171.

[54] W.Q. Bai, L.L. Li, Y.J. Xie, D.G. Liu, X.L. Wang, G. Jin, J.P. Tu, Corrosion and tribocorrosion performance of M (M _ Ta , Ti) doped amorphous carbon multilayers in Hank's solution, Surf. Coat. Technol., 305 (2016), pp. 11–22.

[55] J. Musil, P. Novak, R. Cerstvy, Z. Soukup, Tribological and mechanical properties of nanocrystalline-TiC / aC nanocomposite thin films Tribological and mechanical properties of nanocrystalline-TiC / a -C nanocomposite thin films, J. Vac. Sci. Technol. A., 28 (2010), pp. 244–249.

[56] R. Samiee, B. Ramezanzadeh, E. Alibakhshi, Corrosion inhibition performance and healing ability of a hybrid silane coating in the presence of praseodymium (III) cations, J. Electrochem. Soc., 165 (2018), pp. 777–786.

[57] E. Alibakhshi, M. Ramezanzadeh, S.A. Haddadi, G. Bahlakeh, B. Ramezanzadeh, M. Mahdavian, Persian Liquorice extract as a highly efficient sustainable corrosion inhibitor for mild steel in sodium chloride solution, J. Clean. Prod., 210 (2019), pp. 660–672.

[58] E. Alibakhshi, E. Ghasemi, M. Mahdavian, B. Ramezanzadeh, Fabrication and

characterization of layered double hydroxide/silane nanocomposite coatings for protection of mild steel, J. Taiwan Inst. Chem. Eng., 80 (2017), pp. 924–934.

[59] E. Alibakhshi, E. Ghasemi, M. Mahdavian, B. Ramezanzadeh, A comparative study on corrosion inhibitive effect of nitrate and phosphate intercalated Zn-Al- layered double hydroxides (LDHs) nanocontainers incorporated into a hybrid silane layer and their effect on cathodic delamination of epoxy topcoat, Corros. Sci., 115 (2017), pp. 159–174.

[60] E. Alibakhshi, E. Ghasemi, M. Mahdavian, B. Ramezanzadeh, S. Farashi, Active corrosion protection of Mg-Al-PO_4^{3-} LDH nanoparticle in silane primer coated with epoxy on mild steel, J. Taiwan Inst. Chem. Eng., 75 (2017, pp. 248–262.

[61] E. Alibakhshi, A. Naeimi, M. Ramezanzadeh, B. Ramezanzadeh, M. Mahdavian, A facile synthesis method of an effective anti-corrosion nanopigment based on zinc polyphosphate through microwaves assisted combustion method; comparing the influence of nanopigment and conventional zinc phosphate on the anti-corrosion properties of an epoxy coating, J. Alloys Compd., 762 (2018), pp. 730–744.

[62] E. Alibakhshi, E. Ghasemi, M. Mahdavian, Corrosion inhibition by lithium zinc phosphate pigment, Corros. Sci., 77 (2013), pp. 222–229.

[63] E. Alibakhshi, E. Ghasemi, M. Mahdavian, B. Ramezanzadeh, S. Farashi, Fabrication and characterization of PO_4^{3-} intercalated Zn-Al- layered double hydroxide nanocontainer, J. Electrochem. Soc., 163 (2016), pp. C495–C505.

[64] E. Alibakhshi, E. Ghasemi, M. Mahdavian, Sodium zinc phosphate as a corrosion inhibitive pigment, Prog. Org. Coat., 77 (2014), pp. 1155–1162.

[65] S.A. Haddadi, E. Alibakhshi, G. Bahlakeh, B. Ramezanzadeh, M. Mahdavian, A detailed atomic level computational and electrochemical exploration of the Juglans regia green fruit shell extract as a sustainable and highly efficient green corrosion

inhibitor for mild steel in 3.5 wt% NaCl solution, J. Mol. Liq., 284 (2019), pp. 682–699.

[66] M. Mahdavian, A.R. Tehrani-Bagha, E. Alibakhshi, S. Ashhari, M.J. Palimi, S. Farashi, S. Javadian, F. Ektefa, Corrosion of mild steel in hydrochloric acid solution in the presence of two cationic gemini surfactants with and without hydroxyl substituted spacers, Corros. Sci., 137 (2018), pp. 62–75.

[67] M.J. Palimi, E. Alibakhshi, B. Ramezanzadeh, G. Bahlakeh, M. Mahdavian, Screening the anti-corrosion effect of a hybrid pigment based on zinc acetyl acetonate on the corrosion protection performance of an epoxy-ester polymeric coating, J. Taiwan Inst. Chem. Eng., 82 (2018), pp. 261–272.

[68] M.J. Palimi, E. Alibakhshi, G. Bahlakeh, B. Ramezanzadeh, M. Mahdavian, Electrochemical investigations of the corrosion protection properties of an epoxy-ester coating filled with cerium acetyl acetonate anticorrosive pigment, J. Electrochem. Soc., 164 (2017), pp. C709–C716.

[69] E. Alibakhshi, M. Akbarian, M. Ramezanzadeh, B. Ramezanzadeh, M. Mahdavian, Evaluation of the corrosion protection performance of mild steel coated with hybrid sol-gel silane coating in 3.5 wt.% NaCl solution, Prog. Org. Coat. 123 (2018), pp. 190–200.

[70] E. Alibakhshi, M. Ramezanzadeh, G. Bahlakeh, B. Ramezanzadeh, M. Mahdavian, M. Motamedi, Glycyrrhiza glabra leaves extract as a green corrosion inhibitor for mild steel in 1 M hydrochloric acid solution: Experimental, molecular dynamics, Monte Carlo and quantum mechanics study, J. Mol. Liq., 255 (2018), pp. 185–198.

[71] Y. Chen, J. Zhang, N. Dai, P. Qin, H. Attar, L. Zhang, Corrosion behaviour of selective laser melted Ti-TiB biocomposite in simulated body fluid, Electrochim. Acta., 232 (2017), pp. 89–97.

[72] L. Chen, J. Li, Y. Zhang, L. Zhang, W. Lu, L. Zhang, L. Wang, D. Zhang, Effects of alloyed Si on the autoclave corrosion performance and periodic corrosion kinetics in Zr-Sn-Nb-Fe-O alloys, Corros. Sci., 100 (2015), pp. 651–662.

[73] S. Khamseh, E. Alibakhshi, B. Ramezanzadeh, M.G. Sari, A.K. Nezhad, Developing a Graphite like Carbon:Niobium Thin film on GTD-450 stainless steel substrate, Appl. Surf. Sci. 511 (2020), p. 145613.

[74] R. Samiee, B. Ramezanzadeh, M. Mahdavian, E. Alibakhshi, Assessment of the smart self-healing corrosion protection properties of a water-base hybrid organo-silane film combined with non-toxic organic/inorganic environmentally friendly corrosion inhibitors on mild steel, J. Clean. Prod., 220 (2019), pp. 340–356.

[75] E. Alibakhshi, E. Ghasemi, M. Mahdavian, The effect of interlayer spacing on the inhibitor release capability of layered double hydroxide based nanocontainers, J. Clean. Prod., 251 (2020), p. 119676.

[76] E. Alibakhshi, E. Ghasemi, M. Mahdavian, The influence of surface modification of lithium zinc phosphate pigment on corrosion inhibition of mild steel and adhesion strength of epoxy coating, J. Sol-Gel Sci. Technol., 72 (2014), pp. 359–368.

[77] R. Samiee, B. Ramezanzade, M. Mahdavian, E. Alibakhshi, G. Bahlakeh, Graphene oxide nano-sheets loading with praseodymium cations: Adsorption-desorption study, quantum mechanics calculations and dual active-barrier effect for smart coatings fabrication, J. Ind. Eng. Chem., 78 (2019), pp. 143-154.

[78] P. Qin, Y. Chen, Y. Liy, J. Zhang, L. Chen, Y. Li, X. Zhang, C. Cao, H. Sun, L. Zhang, Resemblance in corrosion behavior of selective laser melted and traditionalmonolithic β Ti- 24Nb-4Zr-8Sn alloy, ACS Biomater. Sci. Eng. Resemblance., 5 (2019), pp. 1141–1149.

[79] R.R. Pareja, R.L. Ibáñez, F. Martín, D. Leinen, Corrosion behaviour of zirconia barrier

coatings on galvanized steel, Surf. Coat. Technol., 200 (2006), pp. 6606–6610.

[80] L. Fedrizzi, F.. Rodriguez, S. Rossi, F. Deflorian, R. Di Maggio, The use of electrochemical techniques to study the corrosion behaviour of organic coatings on steel pretreated with sol–gel zirconia films, Electrochim. Acta., 46 (2001), pp. 3715–3724.

[81] J.P. Holgado, F. Yubero, J.P. Espinos, Corrosion resistant ZrO_2 thin films prepared at room temperature by ion beam induced chemical vapour deposition, Surf. Coat. Technol., 152 (2002), pp. 449–453.

[82] F. Martin, M.C. Lopez, P. Carrera, D. Leinen, XPS depth profile study of porous zirconia films deposited on stainless steel by spray pyrolysis : the problem of substrate corrosion, Surf. Interface Anal., 36 (2004), pp. 8–16.

[83] K. Asami, B.P. Zhang, M. Mehmood, H. Habazaki, K. Hashimoto, Effects of nanoscale heterogeneity on the corrosion behavior of non-equilibrium alloys, Scripta. Mater., 44 (2001), pp. 1655–1658.

[84] S. Khamseh, Synthesis and characterization of tungsten oxynitride films deposited by reactive magnetron sputtering, J. Alloys Compd., 611 (2014), pp. 249–252.

[85] A.A. El-Moneim, B.P. Zhang, E. Akiyama, H. Habazaki, A. Kawashima, K. Asami, K. Hashimoto, The corrosion behaviour of sputter-deposited amorphous Mn-Ti alloys in 0.5 M NaCl solutions, Corros. Sci., 39 (1997), pp. 305–320.

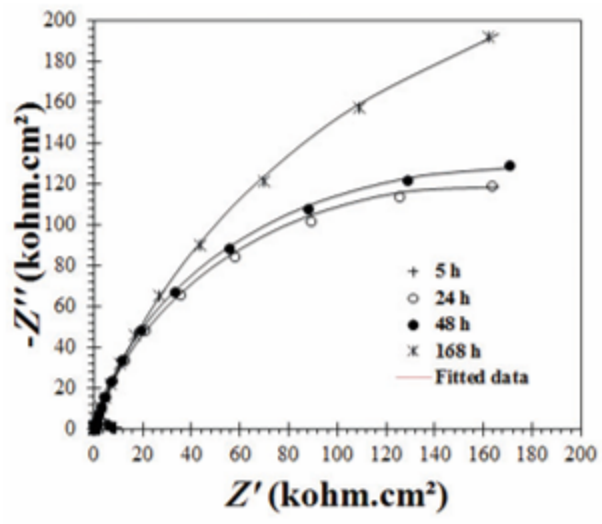
-Z'' (kohm.cm²)
Z' (kohm.cm²)
5 h
24 h
48 h
168 h
Fitted data

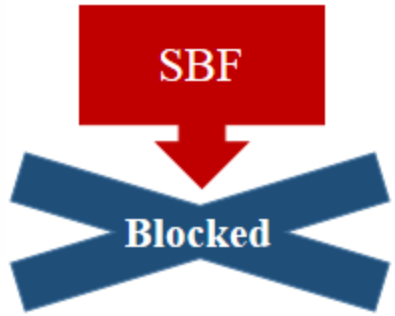
SBF
Blocked

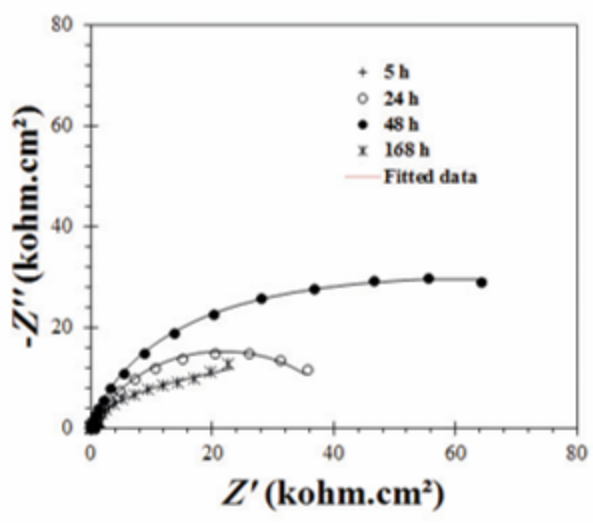
-Z'' (kohm.cm²)
Z' (kohm.cm²)
5 h
24 h
48 h
168 h
Fitted data

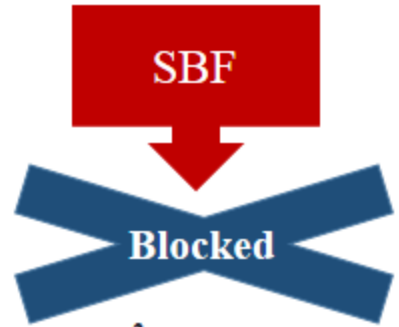
SBF
Blocked


ZrO2
Amorphous structure

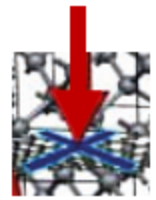
sp2 structure

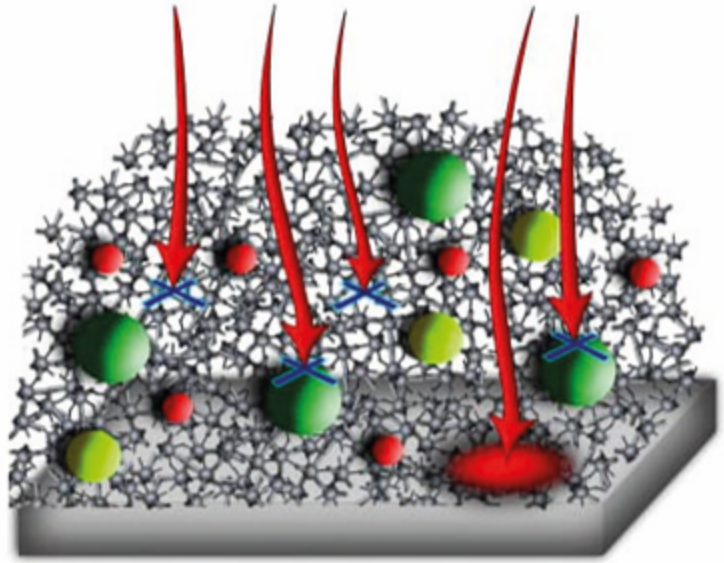

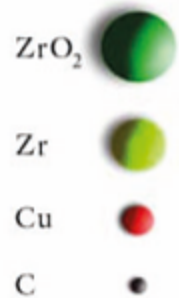
ZrO2
Zr
Cu
C

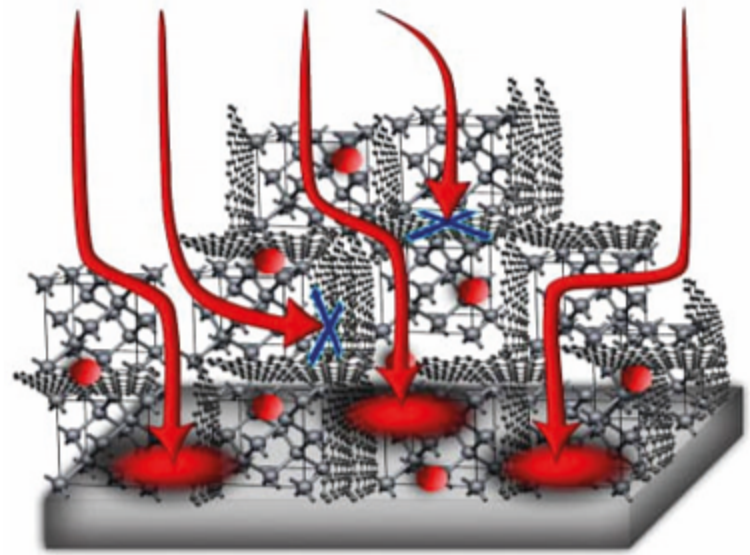

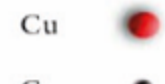
Cu
C